# Simulation Studies of the Electret Effect in Filters

Thesis submitted to the University of Kaiserslautern for the award of the degree of

*MASTER OF SCIENCE*

by

Jitendra Kumar

Supervisors:

Prof. Dr. Dr. h. c. Helmut Neunzert

PD Dr. Arnulf Latz (ITWM)


FACHBEREICH MATHEMATIK
KAISERSLAUTERN, GERMANY

---

August, 2003

## Acknowledgement

It's my privilege to thank my advisor and mentor Prof. Dr. H. Neunzert for his wisdom and generosity. I would like to express my sincere indebted gratitude to Dr. Arnulf Latz for his limitless patience in helping me to accomplish this work.

I am grateful to ITWM and the people attached to it, especially Dr. Heiko Andrä for providing me the necessary facilities during my work. I am also thankful to the Department of Mathematics - Mathematics International of the University of Kaiserslautern for facilitating the studies.

I take this auspicious opportunity to thank my family, friends and well wishers for their constant support and emotional encouragements. Finally, I would like to thank my fiancée Chetna for all her love, support and encouragement.

**Abstract**

In this thesis, we dealt with filtration on a charged fibrous filter. Our aim was to calculate the collection efficiency of a real filter and its dependence on surface charge density of the fibers and particle size. To achieve this goal, the most important aspect was to study the influence of the electric field produced by the fibers on the particle deposition. The filtration efficiency is greatly affected by the nature of airflow through the filter. Thus, our problem can be divided into three different crucial phases.

In the first phase we set up a stationary flow field through the filter. We assembled a group of 12 cylindrical fibers in a systematic way with 2 layers having 6 fibers in each layer as an analogue of a real filter. FEMLAB, a commercial package in MATLAB is used to obtain the flow field through the filter. The airflow is approximated by Stokes flow.

The most important phase of our work was to obtain the electric field across the filter. At the first step we obtained the electric field using FEMLAB, which was cumbersome and time consuming. As the radius of the fiber is very small ($10\mu m$), we proposed a simple idea of approximating the fibers as line charges. This made the calculations very simple and we ended up with simple analytical expressions. The main advantage of this line charge approximation was that we are able to calculate the field without using any software package. In order to get a feeling of the efficiency of this approximation we compare the field with the FEMLAB solution. The fields are nearly concordant with each other. The results obtained from analytical expressions made it possible to approach a solution for sophisticated geometry of the filter. We create a new geometry as a series of straight lines, randomly positioned and oriented in a plane. It was observed that the increase of size of the geometry influences the electric field at a particular point. The magnitude of the field grows with increase in the size and it reaches an asymptotic value. A mathematical proof of this convergence for a simple 2D model has been presented.

The main part of the thesis was to study the motion of aerosol particles. The motion of a particle in a filter is very complicated as it moves under the influence of many forces like electric force, drag force of the air and gravitational force. A mathematical model for the motion and an iterative algorithm for this model has been presented. Capture mechanisms of charged particles as

well as charged polarizable particles are considered.

At last, the theoretical description is outlined to predict the behavior of the particle in the field produced by the fibers. The existence of net repulsive force for polarizable particle upon entering a filter layer is observed. The electric field and the force acting on a moving particle are illustrated. In conclusion, the effectiveness of the filter depending on various filter parameters and the particle size is demonstrated.

# Contents

# Chapter 1

# Introduction

A filter is basically a device for separating one substance from another and filtration is a process of separation. The broad field of solid gas separation is mainly represented as air filters. In this thesis simulation on air filter is being considered. The need for clean air is universal and unlimited. Virtually all-human activities require clean air to survive. Many employees in industry or agriculture need to avoid exposure to airborne particulates and protection is usually provided by respirator filters or large scale filtration units. For this reason, it is no wonder that the history of dust and aerosol filtration is over 2000 years old. One of the most meritorious pioneers in the field of aerosol filtration science, Charles Norman Davies, has described this historical development very extensively up to 1970 [1].

During 1940s-1950s, several types of fibrous materials in the form of soft pads, felt, or papers were tried. It had been found empirically that asbestos, mainly chrysotile and crocydolite, fibers were very effective filtering materials, because of the thinness of the single fibers. After this, asbestos was replaced by other fiber types, mainly by thin glass, carbon, ceramic as well as organic fibers. The filtration efficiency depends also on the fiber diameter; efficiency increases with declining fiber diameter.

At present, a relatively large assortment of very good, highly efficient glass as well as polymer fiber filters is commercially available. Almost 50 aerosol filter producers in different countries in Europe, America, Asia, etc. are registered worldwide [2]

Apart from fibrous filters there exits granular filters, fabric filters, and membrane filters. Granular filters consist of packed beds of roughly isometric particles and which act largely by depth filtration. Fabric filters are made

from textile fibers, which are processed into a relatively compacted form by weaving or felting. Fabric filters are usually cleanable, but their resistance to airflow is relatively high. Fibrous filters usually cannot be cleaned and must be disposed of when spent, but their resistance is low. Membrane filters are made from perforated material or highly compacted fibrous material, usually only a few micrometers thick and acting principally by surface filtration.

With regards to the type of separation, filtration can be divided into surface filtration and depth filtration. On first coming across a fibrous filter one might consider its behavior to be similar to that of a net or a sieve; but though filters and net have the same basic purpose their methods of action are different. The size of the holes is critical, but the thickness of the net is not. Two identical nets in series will not perform better than one, which means that the performance can be understood by considering the surface alone; the process is surface filtration. On the other hand, thick fibrous filters are more efficient than thin ones and no fibrous filter is 100% efficient. A filter can be considered as a large number of layers, each sparsely populated with fibers. Even if a single layer has a very low capture efficiency, the filter as a whole can perform well. This process, particle capture throughout the filter, is termed as depth filtration. Our attention is focused on depth filtration in fibrous filters.

The first stage in the development of aerosol filtration, the "parallel fiber model" - a system of parallel, cylindrical, and regularly arranged fibers [3] were simulated. Almost all properties of this model were treated theoretically and experimentally. Further investigation produced the "fan model filter", which consists of a series of parallel layers of equidistant, parallel fibers, but successive layers are rotated in their one plane through random angles. Nevertheless, in the fan model the dispersion of fibers was perfectly homogeneous. This is not so in real filter in which inhomogeneities arise.

At the end of the 1960s, Fuchs and his co-worker concluded that when the geometric parameters, fiber radius, packing density, and filter thickness are known, then it is possible to calculate the resistance and efficiency of a real fiber filter with sufficient accuracy for practical purpose. Later developments have shown that there still were and still are nonnegligible differences between the structures of real fiber filters and mathematical models.

The aerosol particles, as well as the filter, or both can be electrically charged. This enhances the total collection efficiency of a filter. The first approximation theory was published by Natanson [4] and by Havlicek [5].

The organization of this thesis is as follows:

We begin, in **Chapter 2**, with the nature of airflow through a filter. A mathematical model for this flow is established. Computational procedure in FEMLAB to obtain flow field is described.

**Chapter 3** then presents the equations for the electric field used to solve numerically. Analytical approximation to obtain the electric field is formulated and comparison of numerical and analytical results is demonstrated. The dependence of the electric field on the size of the filter is investigated.

**Chapter 4** describes the mathematical model for the particle motion through the filter. An computational algorithm for this model is developed. Capture mechanism of neutral polarizable as well as charged particles have been considered.

We then proceed, in **Chapter 5**, to discuss the characteristics of the electric field. Filter models used in simulation are described in detail. A concept of penetration velocity of the particles has been presented.

Finally, **Chapter 6**, dealing with the numerical results obtained from the simulation of particles motion, demonstrates the collection efficiency dependence on various filter parameters and particle size.

# Chapter 2

# Mathematical model for fluid flow through the filter

An aerosol particle in a fluid stream tends to move in a straight line because of its inertia. Consequently, as the fluid flow curves around an obstacle, the particle begins moving relative to the fluid and may get deposit on the obstacle. This chapter provides a short description of the nature of airflow through a filter and a mathematical model for this airflow.

## 2.1 Nature of airflow through a filter

The behavior of the airflow through fibers of a filter can be affected by four of its intrinsic properties: its mass or inertia, viscosity, elasticity, and molecular properties.

The pressure drop across a filter is often a very small fraction of the atmospheric pressure. So it is reasonable to assume that the air is incompressible. Air can be treated as a continuous fluid provided that the obstacles in its path are large compared with the mean free path of the air molecules. This means that the molecular effects in airflow can be neglected provided that the fibers are not of submicrometer size. Whether the inertia of the air or its viscosity dominates when air flows past an obstacle depends on the scale of the system and on the velocity of the air. The relative importance of the two effects depends on the size of a dimensionless parameter, the Reynolds number $Re$.

$Re = 2R\rho U/\mu$.
where,

$\rho = 1.229\ kg\,m^{-3}$ is the density of air,
$\mu = 1.73 \times 10^{-5}\ kg\,m^{-1}s^{-1}$ is the coefficient of viscosity,
$R = 10 \times 10^{-6}\ m$ is the radius of the fiber, and
$U = 7.04 \times 10^{-2}\ m\,s^{-1}$ is air velocity.
after substituting these values in the formula we get,
$Re = 0.10$.

The Reynolds number is very small, it means that the flow is dominated by its viscosity. So the airflow through the filter can be well-approximated by Stokes flow.

## 2.2 Steady state stokes flow

The airflow through the filter can be considered as steady state since the flow pattern does not vary with time. The steady state Navier-Stokes equations for the incompressible flow are as follows,

$$\nabla \mathbf{v} = 0, \tag{2.1}$$

$$\rho \mathbf{v}.\nabla \mathbf{v} = -\nabla p + \mu \nabla^2 \mathbf{v}. \tag{2.2}$$

The second and the third terms of the equation(2.2) are the pressure force and the viscous force. The first term is called the inertia force. The ratio of the inertia terms to the viscous terms is of order $2R\rho U/\mu$ (Reynolds number). If the Reynolds number is very small, either because the velocity is very small, or the scale of the flow is very small, or the fluid is very viscous, then it should be possible to neglect the inertia terms. When this is possible, the equations of motion take the form

$$\nabla \mathbf{v} = 0, \tag{2.3}$$

$$\nabla p = \mu \nabla^2 \mathbf{v}. \tag{2.4}$$

The above simplified Stokes equations are linear and therefore easier to solve than the full Navier-Stokes equations. The non-dimensional form of the above stokes equations are,

$$\nabla' \mathbf{v}' = 0, \tag{2.5}$$

$$\nabla' p' = \frac{1}{Re} \nabla'^2 \mathbf{v}', \tag{2.6}$$

where prime denotes the dimensionless quantities. System of equations (2.5) and (2.6) along with no slip boundary condition around the fibers are used to calculate the flow field in the filter.

## 2.3 Computational procedure and results

In order to obtain the solution of the flow across the filter we used FEMLAB, a commercial package available under MATLAB. A brief explanation of the procedure involved in the present work is as follows,

**Model Navigator:** Start FEMLAB from MATLAB and select Incompressible Navier-Stokes model in Physics mode.

**Draw Mode:** First we create a box (domain of numerical computation) of dimension $2.5 \times 2.5 \times 2.5$ centered at the origin $(0, 0, 0)$ and then a group of cylinders (fibers approximation) are drown of radius 0.05 unit and length 1.4 unit as shown in the Figure 2.1. The intercylinder distance is 0.5 unit and distance between two layers is 0.6 unit. To reduce the model geometry as much as possible, we cut the cylinders from the box as we are only interested in flow around the cylinders not inside the cylinders.

**Boundary Mode:** With the geometry drawn, the next task is to set boundary conditions for the objects. We define no-slip boundary condition everywhere except on inflow and outflow side of the box. In our case flow direction (y-direction) is perpendicular to the axes of cylinders. We set $\mathbf{v} = (0, 1, 0)$ for inflow velocity and $p = 0$ for outflow pressure.

**PDE Mode:** In the Navier-Stokes application mode, the material parameters are the fluid density, $\rho$; the dynamic viscosity, $\eta$; and the volume force in $x, y$, and $z$-direction, $F_x, F_y$ and $F_z$. In our scaled model we enter $\eta = 1/Re, Re = 0.1$ in the FEMLAB as the viscosity term. Information on fluid density along with details on length scale, velocity scale, and viscosity are all bundled in the Reynolds number. We set 0 values for the density and the volume forces.

**Mesh Mode:** When solving 3-D Stokes equations, we deal with the dependent variables, $u, v, w, p$. With four dependent variables, the problem gets heavy on the memory. Due to this memory problem we use *Coarser* default mesh settings. The mesh consists of 10960 nodal points and 51544 elements.

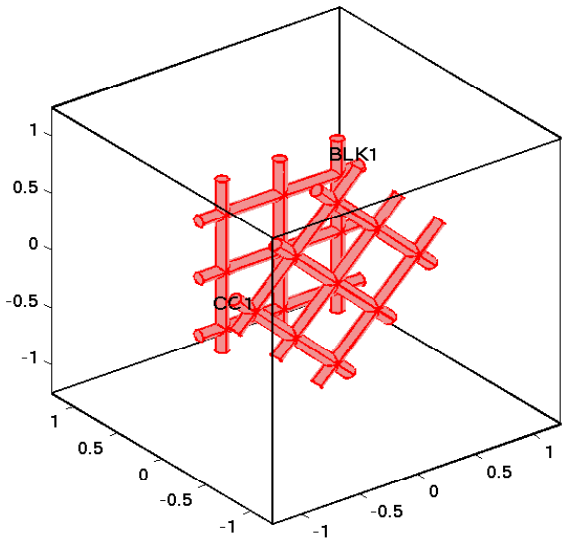


Figure 2.1: Model Geometry

**Solve Mode:** Normally we need not to worry about which solver to use, since an appropriate default solver is chosen by the application mode. But an 'Out of Memory' -problem occurs whenever MATLAB tries to allocate an array, which does not fit sequentially in memory. It is common that the amount of available memory seems large enough for the array but there may exist no continuous block of that size, due to fragmentation. It is important to tune the iterative solver when we have a large number of elements. We use the following parameters in solve mode,

- Sparse null space function (Solve/Parameters/General)
- GMRS iterative solver (Solve/Parameters/Iterative)
- Incomplete LU preconditioning (Solve/Parameters/Iterative)

A steady state velocity field across the filter for the scaled model is obtained. The velocity field through the filter is shown using arrow plot in Figure 2.2. Velocity field $\mathbf{v}$ for the non-scaled model is obtained as follows,

$$\mathbf{v} = \mathbf{v}' \times U$$

where $\mathbf{v}'$ is the velocity of scaled model from FEMLAB and $U$ is the reference Velocity though the filter.

This solution serves as initial flow field for the particle transport. We then use this velocity field to simulate particle-flow in a filter in chapter 3.

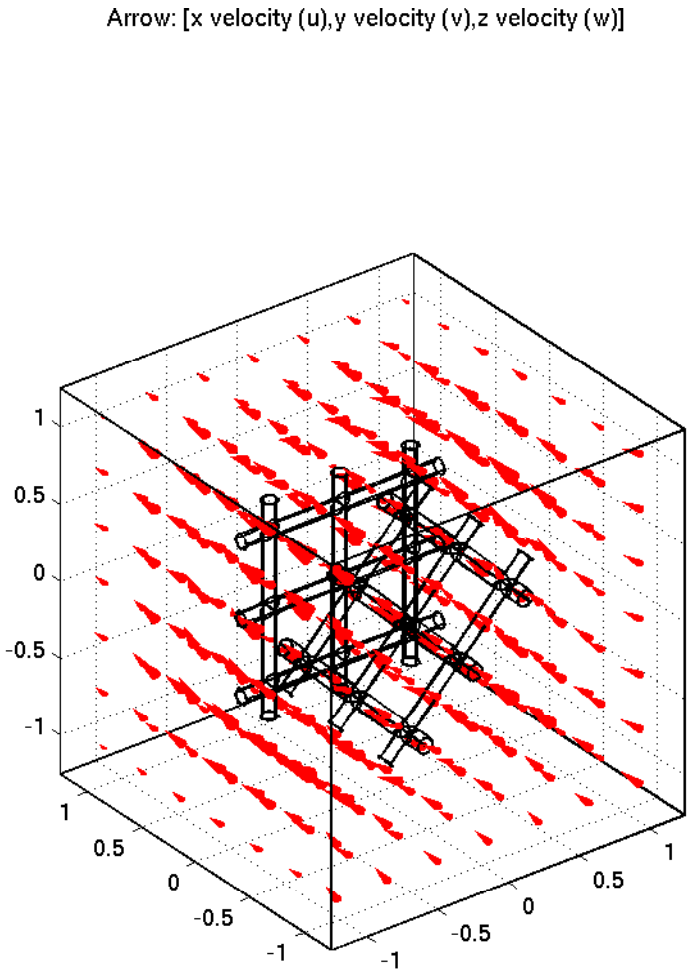


Figure 2.2: Velocity field across the filter

# Chapter 3

# Mathematical model for electric field in the filter

Both the particles and the fibers in the filter may carry electric charges. Deposition of the particles on the fibers may take place because of the forces acting between charges or induced field. This chapter describes a mathematical model for the electric field due to charged fibers (filter). The mathematical model for numerical method and analytical method has been presented. In numerical technique, fibers are assumed to be cylinders and the approximation is limited to 2 layers having 6 fibers in each. As the radius of the fiber is very small ($10\mu m$), we can approximate the fiber with line charge. It makes the calculations very simple and we end up with simple analytical expressions. In analytical technique, an approximation to the filter is considered as a series of straight lines, random in position and orientation, drawn in a plane with some depth (normal to the plane). A filter approximation used in numerical technique and analytical technique is shown in Figure 3.1. Results are compared in both the techniques and they are quite similar.

Due to long range character of the coulomb forces it is expected that there is a strong size dependence of the electric field for small filters. This effect can be studied largely within the analytical solvable model of the filter. Extension of the size of the geometry increases the field in the domain around the fibers. In section 2.3, the existence of the finite electric field in the infinite dimensional filter is analyzed mathematically as well as numerically (Figure3.5). The effects of size of geometry on electric field and comparison of numerical and analytical results have been demonstrated in Figure 3.7.

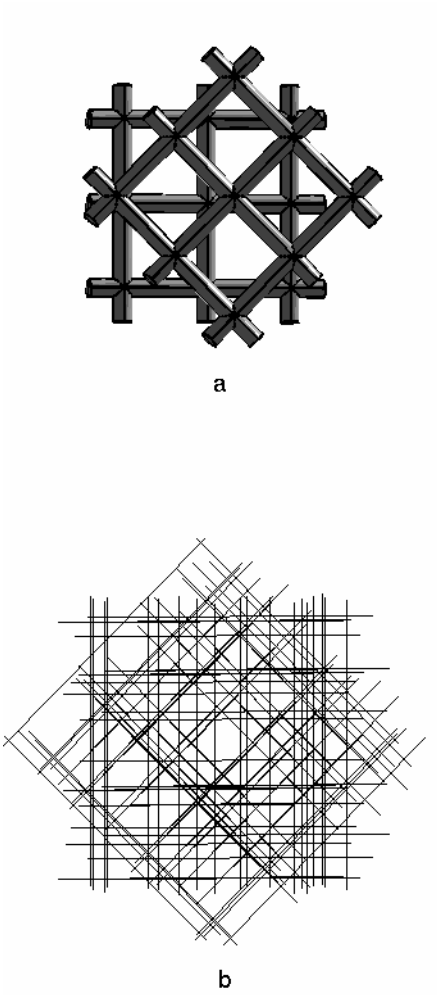


Figure 3.1: Filter appoximation used in (a) Numerical and (b) Analytical technique

## 3.1 Numerical technique

Gauss's law for the electric field says that the electric flux through any closed surface is proportional to the amount of electric charge contained within that surface. Let $V$ be some volume of space, and let $S = \partial V$ be its surface. Then,

$$\int_S \mathbf{E}.d\mathbf{S} = \frac{Q}{\epsilon_0}$$

where $Q$ is the total charge contained in $V$. We can write $Q$ in terms of the charge density $\sigma$ as,

$$Q = \int_V \sigma dV$$

so that Gauss's law becomes,

$$\int_S \mathbf{E}.d\mathbf{S} = \int_V \frac{\sigma}{\epsilon_0}\, dV$$

If we apply the divergence theorem to E,

$$\int_V \nabla.\mathbf{E}\, dV = \int_V \frac{\sigma}{\epsilon_0}\, dV.$$

This is true for any region $V$. The above expression is only possible if,

$$\nabla.\mathbf{E} = \frac{\sigma}{\epsilon_0}. \tag{3.1}$$

Since the electrostatic field is irrotational, it may be expressed as the gradient of a scalar function. We may define an electrostatic potential $\phi$ by the equation,

$$\mathbf{E} = -\nabla\phi. \tag{3.2}$$

The substitution of Eq.(3.2) in Eq.(3.1) leads at ones to Poisson's equation,

$$\nabla^2\phi = -\frac{\sigma}{\epsilon_0}, \tag{3.3}$$

and in a region of zero charge density to Laplace's equation,

$$\nabla^2\phi = 0. \tag{3.4}$$

It is well known that all materials can be divided, as regards their electric properties, in to two classes, conductors and dielectrics. In conductors electric charges are free to move through the material, whereas in dielectrics they are not. Fibers are in general dielectrics. But, since in the technical literature only effective surface charges are given, we treat the fibers as objects where the whole charge is concentrated on their surface. Moreover, it can be assumed that the distribution of charges on their surface is homogeneous.

In a filter basically we have 2 mediums, one is the fiber itself and the other one is the air around the fiber. Now, let $\sigma$ be the surface charge density of the fibers. In both mediums the potential distribution satisfies the Laplace's equation,

$$\nabla^2\phi = 0, \tag{3.5}$$

with the following boundary conditions on the surface of the fiber,

$$\phi = constant$$

and

$$-\epsilon\,\partial\phi/\partial n = \sigma,$$

where $\epsilon$ is the permitivity of the air and n is the outward unit normal vector to the surface of the fiber. Our description follows Landau [6] and Panofsky [7].

## 3.2 Analytically solvable model

In previous section it was shown that the behavior of electrostatic field can be described by

$$\nabla^2\phi = -\frac{\sigma}{\epsilon_0} \tag{3.6}$$

Solution of our problem can be determined analytically if we assume the fiber as line charge of density $\lambda = 2\pi a\sigma$, where $a$ is the radius of the fiber. Let us consider the simplest case of vertical fiber $AB$ of length $2l$ in the plane $y = 0$ as shown in the Figure 3.2.

Suppose the fiber is enclosed by a surface S. So the charge density within the region $V$ enclosed by the surface $S$ is given by

$$f(r) = \begin{cases} \lambda & \text{if point Q lies on the line AB} \\ 0 & \text{elsewhere} \end{cases}$$

The solution of the Poisson equation (3.6) can be generated from Green's theorem:

$$\int_V \left[\phi\nabla^2\psi - \psi\nabla^2\phi\right] d^3x = \int_S \left[\phi\frac{\partial\psi}{\partial n} - \psi\frac{\partial\phi}{\partial n}\right] ds \tag{3.7}$$

The Poisson differential equation for the potential can be converted into an integral equation if we choose a particular $\psi$, namely $1/R \equiv 1/(|\mathbf{r} - \mathbf{r}'|)$, where $\mathbf{r}$ is the observation point and $\mathbf{r}'$ is the integration variable. Making use of $\nabla^2\phi = -f(r)/\epsilon_0$ and the standard result $\nabla^2(1/R) = -4\pi\delta(\mathbf{r} - \mathbf{r}')$, the equation (3.7) becomes,

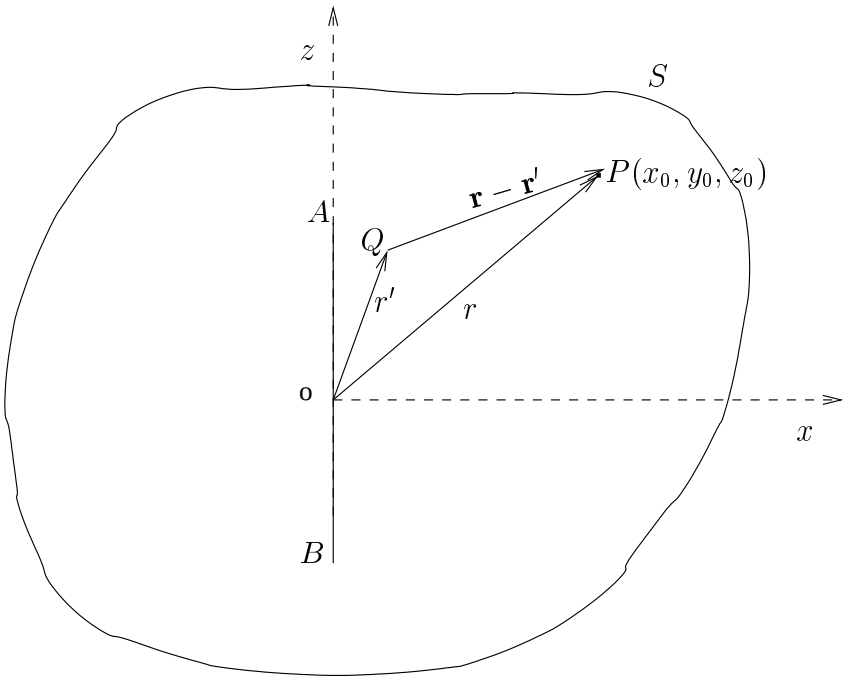


Figure 3.2: Positively charged line AB

$$\int_V \left[-4\pi\delta(\mathbf{r}-\mathbf{r}')\phi(\mathbf{r}') + \frac{1}{R}\frac{f(\mathbf{r}')}{\epsilon_0}\right] d^3r' = \int_S \left[\phi\frac{\partial}{\partial n'}\left(\frac{1}{R}\right) - \frac{1}{R}\frac{\partial\phi}{\partial n'}\right] ds'$$

if $\mathbf{r}$ lies within the volume $V$, we obtain:

$$\phi(\mathbf{r}) = \frac{1}{4\pi\epsilon_0}\int_V \frac{f(\mathbf{r}')}{R} d^3r' + \frac{1}{4\pi}\int_S \left[\frac{1}{R}\frac{\partial\phi}{\partial n'} - \phi\frac{\partial}{\partial n'}\left(\frac{1}{R}\right)\right] ds' \tag{3.8}$$

If the surface $S$ goes to infinity then the surface integral vanishes and equation (3.8) reduces to,

$$\phi(\mathbf{r}) = \frac{1}{4\pi\epsilon_0}\int_V \frac{f(\mathbf{r}')}{R} d^3r'$$

or

$$\phi(x_0, y_0, z_0) = \frac{1}{4\pi\epsilon_0}\int_{-l}^{l} \frac{\lambda}{\sqrt{x_0^2 + y_0^2 + (z_0 - z)^2}} dz \tag{3.9}$$

making some transformations and using some standard integrals the above integral can be simplified as

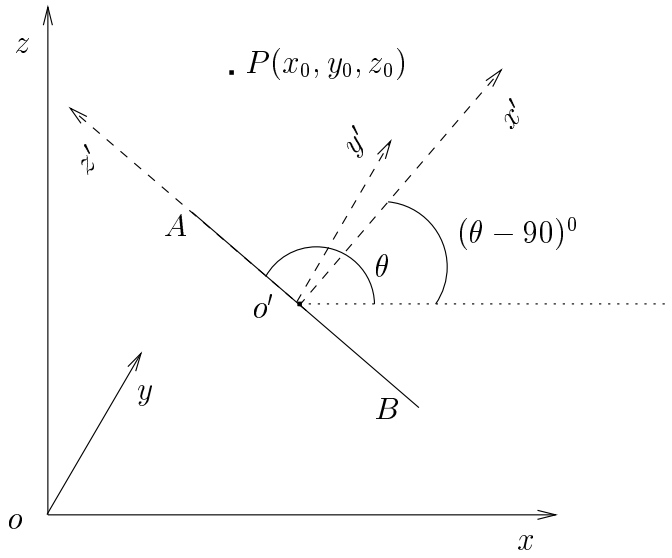


Figure 3.3: Positively charged line AB

$$\phi(x_0, y_0, z_0) = \frac{\lambda}{4\pi\epsilon_0} \log \frac{(z_0 + l) + \sqrt{x_0^2 + y_0^2 + (z_0 + l)^2}}{(z_0 - l) + \sqrt{x_0^2 + y_0^2 + (z_0 - l)^2}} \tag{3.10}$$

The electric potential due to any arbitrary vertically oriented line can be calculated by applying appropriate translation and rotation of the coordinate axes. Consider two sets of rectangular Cartesian frames of reference $o - xyz$ and $o' - x'y'z'$ as shown in the Figure 3.3. Let us consider a line $AB$ which is oriented in the plane $y = b$ at an angle $\theta$. The frame of reference $o' - x'y'z'$ is obtained by shifting of the origin and rotating $ox$ and $oz$ through an angle $(\theta - 90)$ in the counter-clockwise direction. If an arbitrary point $P$ has coordinate $(x_0, y_0, z_0)$ and $(x_0', y_0', z_0')$ with respect to $o - xyz$ and $o' - x'y'z'$ respectively and the coordinate of $o'$ (mid point of the line) with respect to $0 - xyz$ is $(a, b, c)$, then

$$\begin{aligned} x_0' &= (x_0 - a)cos(\theta - 90) + (z_0 - c)sin(\theta - 90) \\ y_0' &= (y_0 - b) \\ z_0' &= -(x_0 - a)sin(\theta - 90) + (z_0 - c)cos(\theta - 90) \end{aligned}$$

or

$$\begin{aligned} x_0' &= (x_0 - a)sin(\theta) - (z_0 - c)cos(\theta) \\ y_0' &= (y_0 - b) \\ z_0' &= (x_0 - a)cos(\theta) + (z_0 - c)sin(\theta). \end{aligned}$$

Now, the electric potential $\phi$ at $P$ due to an arbitrary line is given by

$$\phi(x_0', y_0', z_0') = \frac{\lambda}{4\pi\epsilon_0} \log \frac{(z_0' + l) + \sqrt{x_0'^2 + y_0'^2 + (z_0' + l)^2}}{(z_0' - l) + \sqrt{x_0'^2 + y_0'^2 + (z_0' - l)^2}} \tag{3.11}$$

by substituting the values of $x_0', y_0', z_0'$ in terms of $x_0, y_0, z_0$ in equation (3.11) we get the required potential. We can define electric field $\mathbf{E}$ by the equation

$$\mathbf{E} = -\nabla\phi. \tag{3.12}$$

Equation (3.12) leads to the following expressions for the components of the electric field in the simplest case of a vertical line,

$$E_x = \frac{k\lambda x_0}{(x_0^2 + y_0^2)} \left[ \frac{z_0 + l}{\left\{x_0^2 + y_0^2 + (z_0 + l)^2\right\}^{1/2}} - \frac{z_0 - l}{\left\{x_0^2 + y_0^2 + (z_0 - l)^2\right\}^{1/2}} \right]$$

$$E_y = \frac{k\lambda y_0}{(x_0^2 + y_0^2)} \left[ \frac{z_0 + l}{\left\{x_0^2 + y_0^2 + (z_0 + l)^2\right\}^{1/2}} - \frac{z_0 - l}{\left\{(x_0^2 + y_0^2 + (z_0 - l)^2\right\}^{1/2}} \right]$$

and

$$E_z = k\lambda \left[ \frac{1}{\left\{x_0^2 + y_0^2 + (z_0 - l)^2\right\}^{1/2}} - \frac{1}{\left\{x_0^2 + y_0^2 + (z_0 + l)^2\right\}^{1/2}} \right]$$

where $k = 1/(4\pi\epsilon_0)$.

In order to get $\mathbf{E}(E_x, E_y, E_z)$ for a group of line charges: $(a)$ Calculate $\mathbf{E}_n$ due to each line charge at the given point as if it were the only line present. $(b)$ Add these separately calculated fields vectorially to find the resultant field $\mathbf{E}$ at the point. In equation form,

$$\mathbf{E} = \mathbf{E_1} + \mathbf{E_2} + \mathbf{E_3} + \cdots = \sum \mathbf{E_n} \qquad n = 1, 2, 3, \ldots$$

The sum is a vector sum, taken over all the line charges.

In order to calculate the electric field in the filter, we considered only four types of line charges. Two of them are aligned to x and y axes and the other two are oriented at $45^0$ and $135^0$ with respect to x-axis. These lines are drown randomly in a 3-dimensional space with interfiber distance of $100\,\mu m$ and spacing between two layers as $120\,\mu m$.

## 3.3 Existence of finite electric field

Analytical formulation describes above follows an idea to extend the filter geometry. We extend the filter geometry by adding more line charges in the existing line charge approximation. The extension in the size of the filter comes up with an increasing behavior of the field. It was important to look for the appropriate dimension of the filter to work with. We make a convergent test. We calculated the field at some arbitrary points around the filter geometry by increasing the size of the geometry. It was observed that the increment in size of the filter influences the field. From a certain finite size, no changes in the electric field could be observed anymore. We fixed this size as the size of our filter to obtain the electric field. In our case it is $0.3\,m$. Figure 3.4 shows the effect of the size of the filter on electric field at a point near to the center.

In order to analyze the convergence of the electric field analytically, the following assumptions have been made for simplicity,

- Filter has only one layer
- Only horizontal and vertical fibers are considered
- Interfiber distance in each direction ($x$ or $z$) is equal

Let $(2N + 1)$ and $(2M + 1)$ are the number of fibers in $x$ and $z$ direction. The space between the fibers in x and z direction are denoted by $\Delta x$ and $\Delta z$ respectively. Clearly from the Figure 3.5, the length of the horizontal and the vertical fibers is given by $2N\Delta x$ and $2M\Delta z$ respectively. Let $P(x_0, y_0, z_0)$ be an arbitrary point around the filter. For the filter of large dimension, the x component of the electric field at $P$ can be formulated as

$$E_x = V + H$$

where

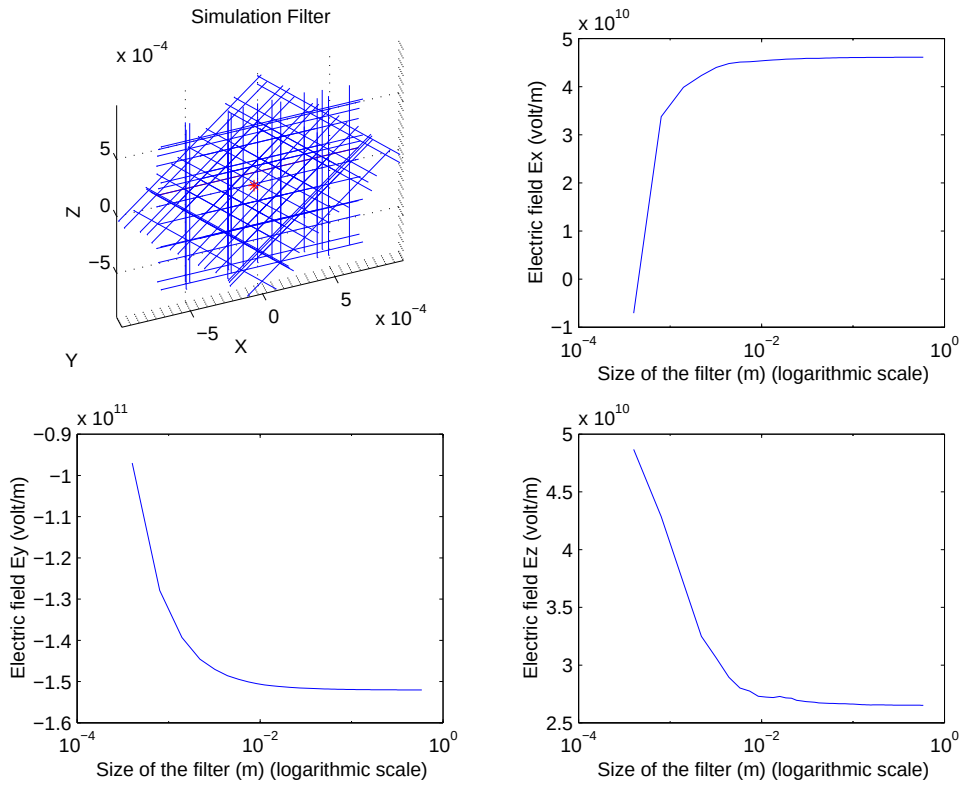


Figure 3.4: Size effect at the point $(-6 \times 10^{-5}, -7 \times 10^{-5}, 8 \times 10^{-5})$

$$V = lim_{M,N\to\infty} \sum_{n=-N}^{N} \left[ \frac{k\lambda(x_0 - n\Delta x)}{(x_0 - n\Delta x)^2 + y_0^2} \left\{ \frac{z_0 + M\Delta z}{\{(x_0 - n\Delta x)^2 + y_0^2 + (z_o + M\Delta z)^2\}^{1/2}} - \frac{z_0 - M\Delta z}{\{(x_0 - n\Delta x)^2 + y_0^2 + (z_o - M\Delta z)^2\}^{1/2}} \right\} \right] \quad (3.13)$$

and

$$H = lim_{M,N\to\infty} \sum_{n=-M}^{M} \left[ k\lambda \left\{ \frac{1}{\{(x_0 - N\Delta x)^2 + y_0^2 + (z_o - m\Delta z)^2\}^{1/2}} - \frac{1}{\{(x_0 + N\Delta x)^2 + y_0^2 + (z_o - m\Delta z)^2\}^{1/2}} \right\} \right] \quad (3.14)$$

for large $N(N \to \infty)$ and $M(M \to \infty)$ we can assume that

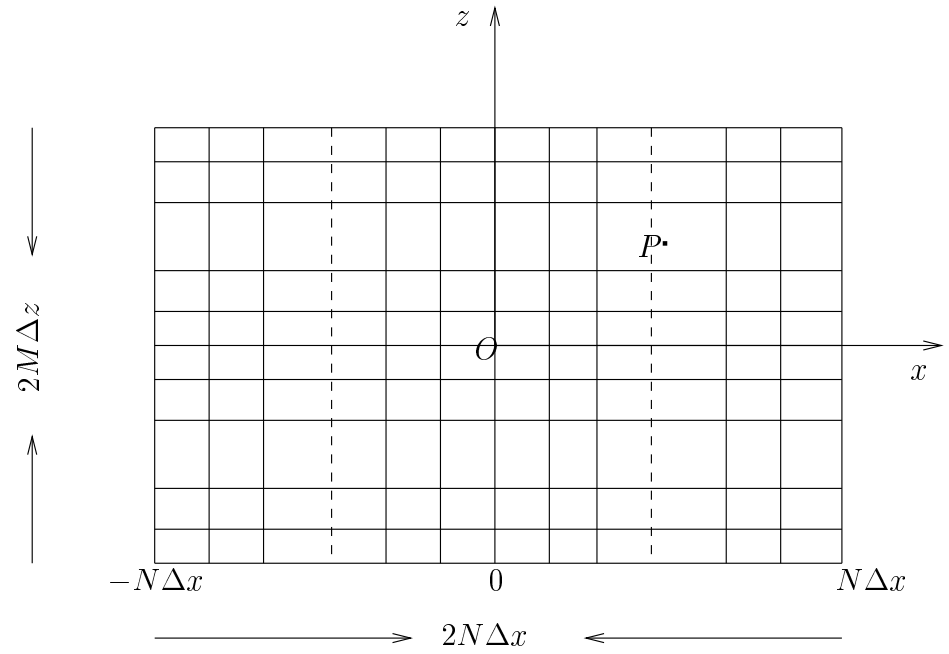


Figure 3.5: Filter approximation for analytical analysis

$$(x_0 - N\Delta x)^2 \approx (x_0 + N\Delta x)^2 \approx N^2\Delta x^2$$

and

$$(z_0 - M\Delta z)^2 \approx (z_0 + M\Delta x)^2 \approx M^2\Delta x^2$$

after substituting these approximations in equations (3.13) and (3.14) we get

$$E_x = lim_{M,N\to\infty} \sum_{n=-N}^{N} f_n \tag{3.15}$$

where

$$f_n = \frac{2k\lambda(x_0 - n\Delta x)M\Delta z}{\{(x_0 - n\Delta x)^2 + y_0^2\}\{(x_0 - n\Delta x)^2 + y_0^2 + M^2\Delta z^2\}^{1/2}}.$$

Equation (3.15) can be rewritten as,

$$E_x = lim_{M,N\to\infty} \sum_{n=1}^{N} (f_n + f_{-n}) + constant$$

or

$$E_x = lim_{M\to\infty} \sum_{n=1}^{N} (f_n + f_{-n}) + lim_{M\to\infty} \sum_{n=N}^{\infty} (f_n + f_{-n}) + constant \quad (3.16)$$

or

$$E_x = I_1 + I_2 + constant$$

Clearly, $I_1$ is finite, and for the $I_2$ we can have the same assumptions as before,

$$(x_0 - n\Delta x)^2 \approx (x_0 + n\Delta x)^2 \approx n^2\Delta x^2$$

for sufficiently large n. Thus, we have

$$I_2 = lim_{M\to\infty} \sum_{n=1}^{\infty} \frac{2k\lambda(2x_0)M\Delta z}{\{n^2\Delta x^2 + y_0^2\}\{n^2\Delta x^2 + y_0^2 + M^2\Delta z^2\}^{1/2}}$$

$$= \sum_{n=1}^{\infty} \frac{4k\lambda x_0\Delta z}{\{n^2\Delta x^2 + y_0^2\}}.$$

since $I_2$ is a convergent series the electric field $E_x$ must converge to some value. The convergence of $E_y$ and $E_z$ can be shown in the similar way.

## 3.4 Comparison of numerical and analytical results

We have numerical and analytical techniques to obtain the electric field across the filter. As we have mentioned above, in numerical technique we are limited to very few fibers in the model filter. In previous section we have analyzed that the dimension of a filter influences the electric field. So, it is not a good idea to take just 8-12 fibers in a simulation filter.

To compare the results of both the techniques, we created rather simple model geometry of a filter having 2 layers and 4 fibers in each. The electric field using numerical technique is calculated by FEMLAB. In the similar way as we calculated the flow field in the last chapter, the computational procedure is as follows,

- First create a geometry model as in Figure 3.6.

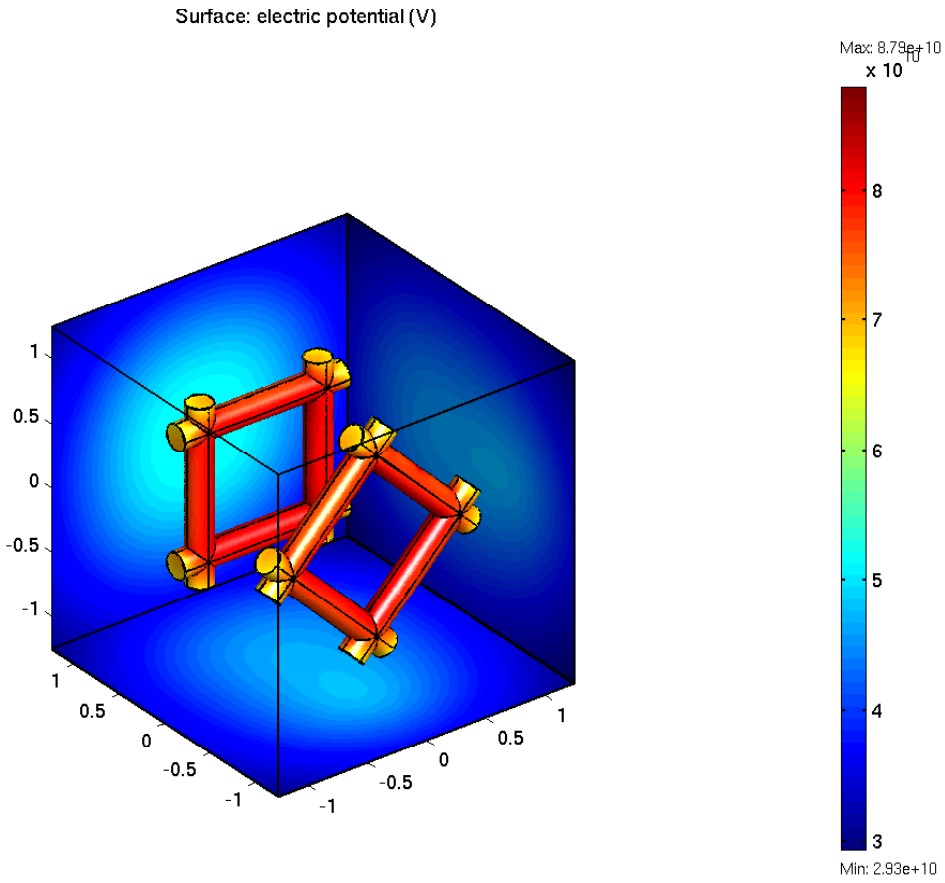


Figure 3.6: Electric potential across a filter

- Set boundary condition $\rho_s = 1$ around the fibers for the surface charge density and potential $V$ on the surface of the computational domain. The potential due to fibers was calculated by approximating cylinders as line charges.
- In subdomain setting, we set zero value for space charge density in both the regions and leave the default setting for other parameters.
- Initialize the mesh and solve the model using *Good Broyden* iterative solver and *Algebraic Multigrid* preconditioner.

The magnitude of the electric field at some arbitrary points in the domain has been calculated using both FEMLAB and analytical techniques for the same model filter. Line charge approximation of the cylinders considered in

the analytical technique. Results are compared in Figure 3.7. The results show that the electric fields for the model filter are quite similar. The figure also shows the results for the electric field, if more line charges are added until the electric field has reached its asymptotic value.

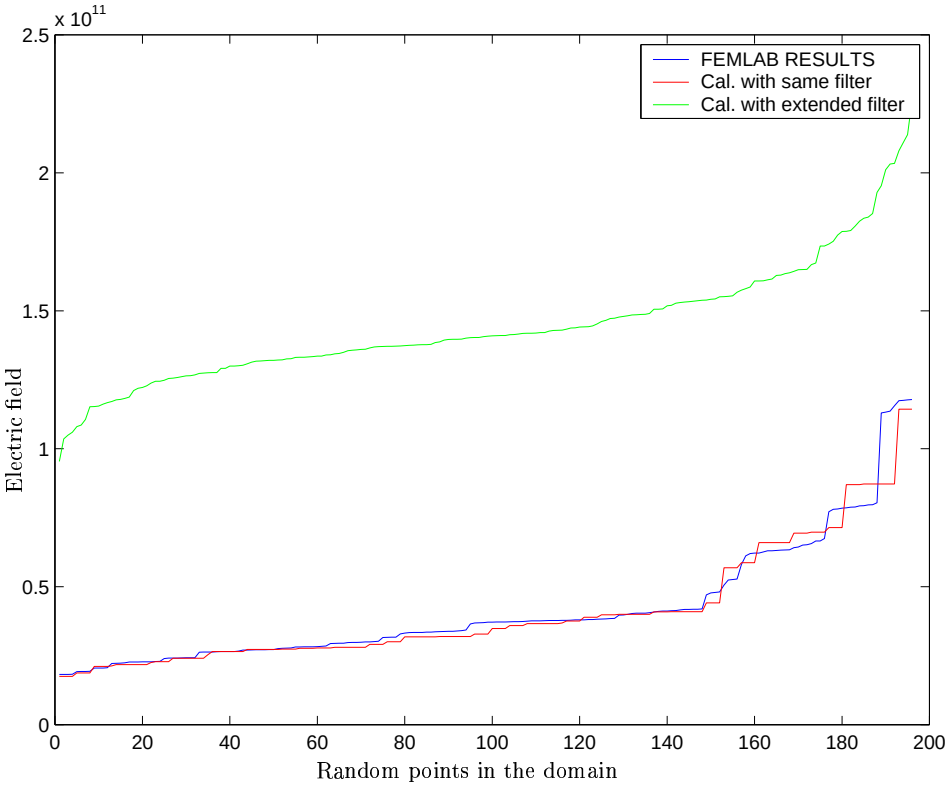


Figure 3.7: Comparision of analytical and numerical results

# Chapter 4

# Numerical simulation of particle motion in the filter

This chapter deals with the numerical simulation of particle motion through filters. A numerical solution concept is presented which appears well suited to study the particle transport, deposition and influence on the motion of the charged and neutral particle by the filter material caring an electric charge.

## 4.1 Introduction

Fibers of different kind are used for extraction of a solid phase from a gas phase. The geometric and physical properties of two-phase flow in realistic filter configuration are usually so complex that in practice filter performance is estimated by empirical or semiempirical relations only. However, for prediction and improvement of filter performance, detailed knowledge of internal two phase flow and, in particular, of its interaction with the filter material is essential.

Filter material carrying an electric charge is widely used in particulate respirator capsules and disposable filtering face pieces, but it also has a place in vacuum cleaners, air conditioning units, and filters on large scale. The advantage of the material is that it functions by means of an attractive force between airborne particles and filter fibers, which augments filtration efficiency without any penalty of increased airflow resistance.

The greater part of the mass of most aerosols consists of electrically charged particles, but all particles respond to an electric field by means of induced dipole forces. In this work particles of diameter of the order of $1\mu m$ are

considered.

The computation of this interactive flow problem results in an iterative procedure between fluid flow, particle transport, deposition and electric field produced by the fibers. The simulation of the filter flow requires, therefore, modeling and solution of four essential parts, of the particle motion, of the deposition, of the flow field and of the electric field. The computation of the airflow field and the electric field produced by the fibers have already been described in chapter 2 and chapter 3.

The deposition of particles is of complex nature; it depends in principle on intermolecular forces. Its detail description is not being considered in this report; therefore a rather simple model is used, which assumes any particle as deposited if it has touched the fiber.

## 4.2 Mathematical model for the particle motion

Particles with the diameter in the order of $1\mu m$ are considered as solid sphere in the dilute concentration. They are treated as individual particles. Let $\mathbf{r}(t)$ be the position vector of a particle at time $t$. The velocity of the fluid and the particle is denoted by $\mathbf{v}$ and $\mathbf{u}$ respectively. Thus the motion of the particle is described by the equations,

$$\frac{d\mathbf{r}}{dt} = \mathbf{u} \tag{4.1}$$

$$\frac{d\mathbf{u}}{dt} = \alpha(\mathbf{v} - \mathbf{u}) + \frac{\mathbf{F}_{ext}}{m_p} \tag{4.2}$$

with initial conditions: $\mathbf{u}(0) = \mathbf{u}_0$ and $\mathbf{r}(0) = \mathbf{r}_0$

where

$$\alpha = \frac{3}{8}\frac{\rho_f}{\rho_p r_p} c_d \left|\mathbf{u}(t) - \mathbf{v}\left(\mathbf{r}(t)\right)\right|, \quad c_d = f(Re_p), \quad Re_p = \frac{2r_p|\mathbf{u} - \mathbf{v}|}{\nu}$$

$r_p$ is the particle radius, $\nu$ is the fluid viscosity, $m_p$ is the mass of the particle, and $\rho_p$, $\rho_f$ are the densities of the particle and the fluid respectively. The drag coefficient of the spherical particles is linear in velocity and is described by the Stokes formula $c_d = 24/Re_p$ for $Re_p$ less than 0.1. So $\alpha$ can be rewritten as,

$$\alpha = \frac{9\,\nu\,\rho_f}{2\,\rho_p\,r_p^2}$$

$F_{ext}$ is the external force i.e., the force due to electrically charged fiber material in our case. In this study we have divided our investigations into two phases. The first phase is concerned with the effects of charged fibers on the filtration efficiency of an initially charged particle. The second phase is concerned with the effect of charged fibers on the efficiency of filtration of neutral polarizable aerosol particles.

### 4.2.1 Capture of charged particles

The electrical mechanism of removal in a fibrous filter is related to the electrostatic force between the aerosol and the fibers. This force may be either a Coulomb or a polarization force. The Coulomb force exerted on an aerosol particle possessing a charge $q_p$ in an electric field of intensity $E$ surrounding a charged fiber is as follows,

$$\mathbf{F}_c = q_p\,\mathbf{E}$$

If $F_c$ is negative, the particle tends to move from the aerosol stream onto the fibers, the net effect being an increase in filtering efficiency. Conversely, a positive value would indicate a lowering of efficiency.

The computation of the field $\mathbf{E}$ has been evaluated in chapter 3. Aerosol charge can take a wide range of values, depending on circumstances. A typical value of charge that a aerosol particle with a diameter $d_p$ can hold is $n_q$ fundamental charges, where,

$$n_q = 10.1\,d_p^{1.2}.$$

### 4.2.2 Capture of neutral particles

An electric field will influence a particle that has no charge of its own because the constituent material of the particle will be polarized by the electric field, which will then attract the induced dipole. The magnitude of the electric dipole is proportional to the electric field strength at the position of the particle and to the particle volume, and it also depends on the dielectric constant of the material making up the particle. The electric field due to a charged fiber falls off with increasing distance, and so the attracted part of the dipole will be in a slightly higher field than the repelled part. The result

of this slight imbalance is a net attractive force on the particle. The force on a particle caused by polarization is given as,

$$\mathbf{F}_p = \frac{\pi d_p^3 \epsilon_0}{4} \left( \frac{D_p - 1}{D_p + 2} \right) \nabla(\mathbf{E}^2)$$

i.e., the force depends also on the gradient of the field in addition to the field itself. The motion of the particle will be in direction of the greatest field strength, that is, towards the fiber.

Thus, the total external force on a charged dielectric particle is the sum of Coulomb and Polarization force, that is,

$$\mathbf{F}_{ext} = \mathbf{F}_c + \mathbf{F}_p$$

## 4.3 Simulation algorithm

As we have seen in the last section the equations of the particle motion require the velocity field for the air and the electric field. The velocity field and the electric field have been calculated in chapter 2 and chapter 3. The electric field can be obtained at any point in the domain, but on the contrary the velocity field is given at some grid points in the domain. The implementation of the algorithm for the motion of the particle works by the combination of numerical and analytical solution of the equations of motion. The time steps are taken adaptively. The following are the main steps used to describe the motion of the particle.

1. Define a time step $\Delta t = d/u_0$, where $d \in \mathbb{R}$ is smaller than the diameter of the fiber.

2. Compute $\mathbf{r}_1 = \mathbf{r}_0 + \mathbf{u}_0 \, \Delta t$.

3. Calculate the electirc field at $\mathbf{r}_1$ and then the total external force $\mathbf{F}_{ext}$ applied on the particle.

4. Obtain the velocity field $\mathbf{v}$ of the air at the nearest grid point of $\mathbf{r}_1$.

5. Compute the solution of the following differential equation for the time step $\Delta t$ keeping $\mathbf{v}$ and $\mathbf{F}_{ext}$ as constants

$$\frac{d\mathbf{u}}{dt} = -\alpha \, \mathbf{u} + \alpha \, \mathbf{v} + \frac{\mathbf{F}_{ext}}{m_p}$$

as

$$\mathbf{u}_1 = \left(\mathbf{v} + \frac{\mathbf{F}_{ext}}{\alpha\, m_p}\right) + \left(\mathbf{u}_0 - \mathbf{v} - \frac{\mathbf{F}_{ext}}{\alpha\, m_p}\right) e^{-\alpha\, \Delta t}$$

6. update $\mathbf{u}_0 = \mathbf{u}_1$ and $\mathbf{r}_0 = \mathbf{r}_1$.

7. Iterate steps 1 to 6 until the particle gets trapped on the fiber or leaves the filter.

# Chapter 5

# Characteristics of the electric field across the filter

In this chapter attention is focused on the theoretical description of the behavior of the particle motion in the field produced by the filter. The filter approximations used in the simulation are introduced. The most basic finding of this chapter is to observe the electric field behavior due to the filter. The electric field as we move towards the filter is demonstrated in section 5.2. For simplicity the electric field for two parallel line charges is calculated and it has been compared with the field behavior observed in a real model filter. The field behavior with particle motion in the filter has also been presented. In the whole discussion, we assumed that the fibers are positively charged and the particles are negatively charged.

## 5.1 Model filter used in simulation

Here we describe the models used in simulation and their approximations to obtain the solution of different phases of the problem. Let us first look at the simulation filter used in the motion of the particle. We designed a group of 12 cylinders in a systematic way with 2 layers having 6 cylinders in each as shown in the Figure 5.1. One layer is fixed exactly above the plane of the other and is rotated by an angle of $45^0$.

The Electric field and the airflow field are required for the final simulation of aerosol particle motion. The stationary airflow field was calculated on this cylindrical model. The calculations of electric field were done on two different models. In first model we approximate the cylinders as line charges. We called this model as primary model (Figure 5.2 (a)). In second model,

more lines are added around the primary model until the field converges (see chap. 3). We can call this model as extended model (Figure 5.2 (b)). The primary model was kept as such in the extended model, since the flow field is calculated only for cylindrical model. Evidently, it is too time consuming to calculate the field in the extended model, but it is a better realization of the real filter. The field inside the extended model is very complex as the line charges are also added randomly in depth whereas in primary model it was very symmetric.

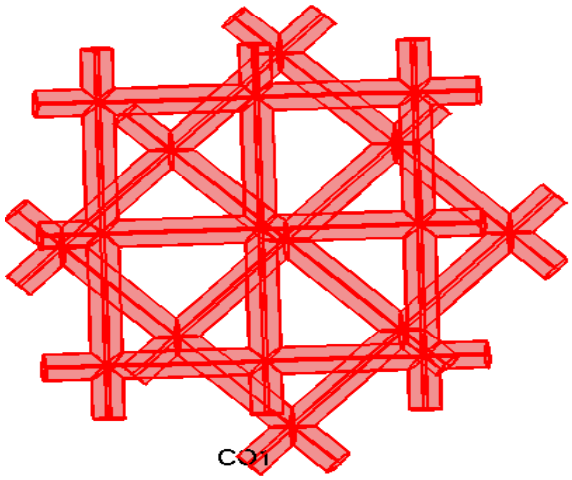


Figure 5.1: Cylinderical fiber model

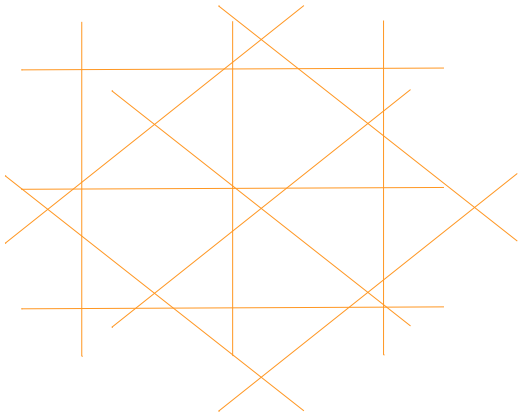

(a) Primary model

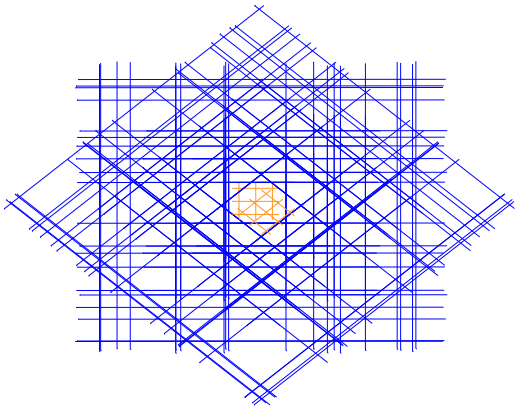

(b) Extended model

Figure 5.2: Models used to calculate the electric field

## 5.2 Electric field across the filter

In this work we consider a filter consisting of two layers, placed in $xz$ plane. We are looking for the field behavior away from the filter in $y$ direction. The field distribution changes, if there is a change in the starting point on the $xz$ plane. We check this for different starting point and observe an interesting behavior of the field shown in Figure 5.3.

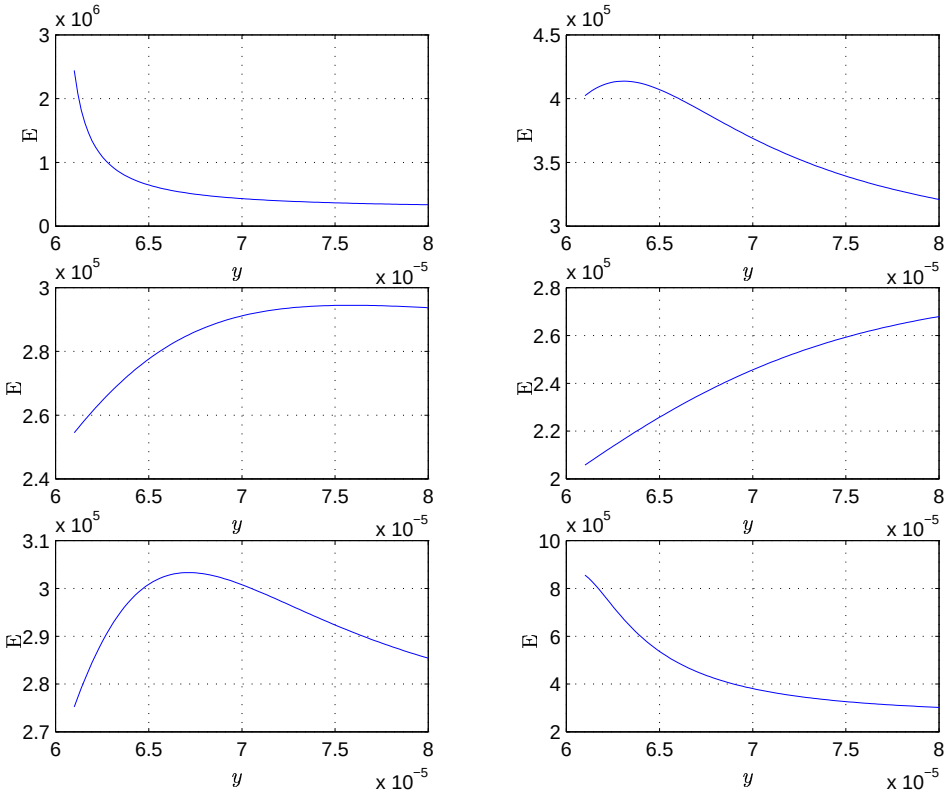


Figure 5.3: Electric field variation in a direction normal to the filter plane. Different curves are for different starting positions on the filter plane

The field decreases as we go away from the filter, but for certain starting points the field behaves differently. It increases till a point (close to the filter) and after that we get the normal decreasing behavior. The curves shown in Figure 5.3 are for various starting points on the $xz$ plane.

The gradient of the field for corresponding starting positions are shown in Figure 5.4. In the last chapter we have seen that the polarization force depends on the gradient of the field rather than on the field. A particle would

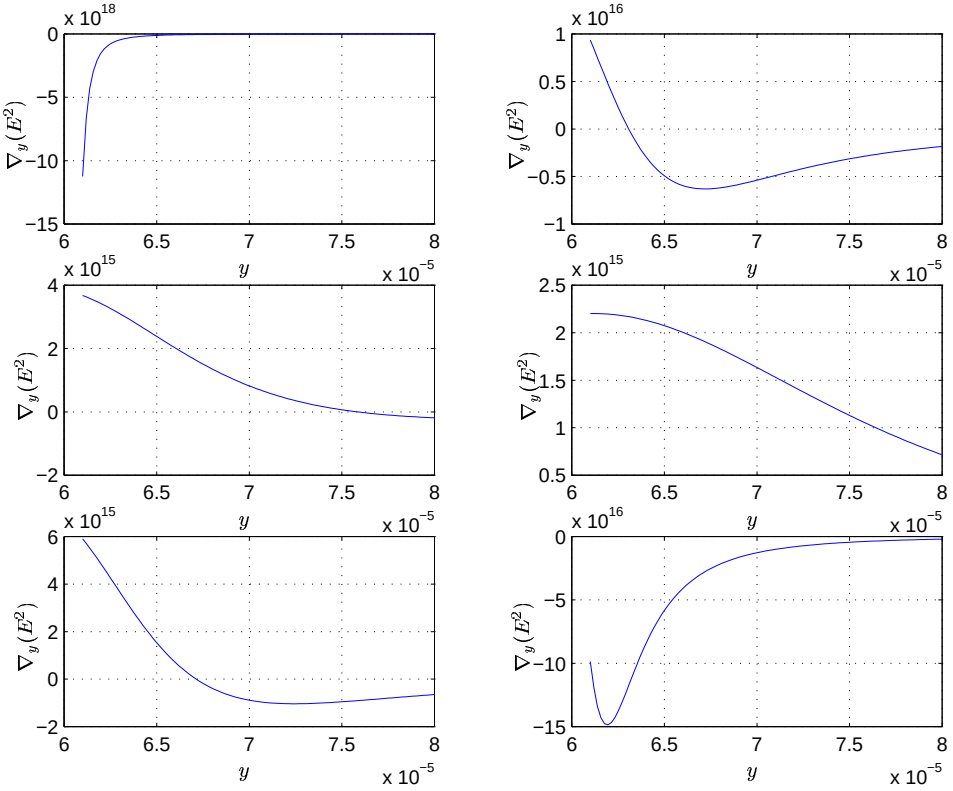


Figure 5.4: Gradient of $E^2$

feel a repulsive force either it leaves the filter at a point where the gradient is positive or enters at a point where the gradient is negative.

As the electric field behavior is very complicated for the model filter, we take a simple case of two line charges of length $0.3\,m$ in $xz$ plane as shown in Figure 5.5. We observe the electric field behavior as we move in y direction away from the plane. We calculated the field values for different $x$ positions keeping $z$ fixed. There was no change in the field behavior close to the center of the line. Although for finite length, the two lines are not strictly translational invariant in the $x$ direction. Figure 5.6 shows the variation of electric field in $y$ direction starting from 6 different points in $xz$ plane. $x$ varies from $-40\,\mu m$ to 0 for a fixed $z$.

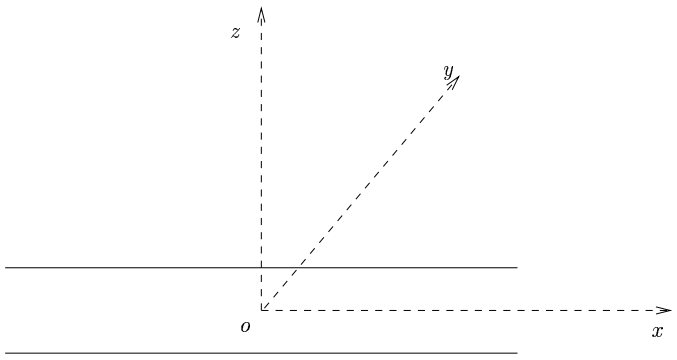


Figure 5.5: 2 line charges

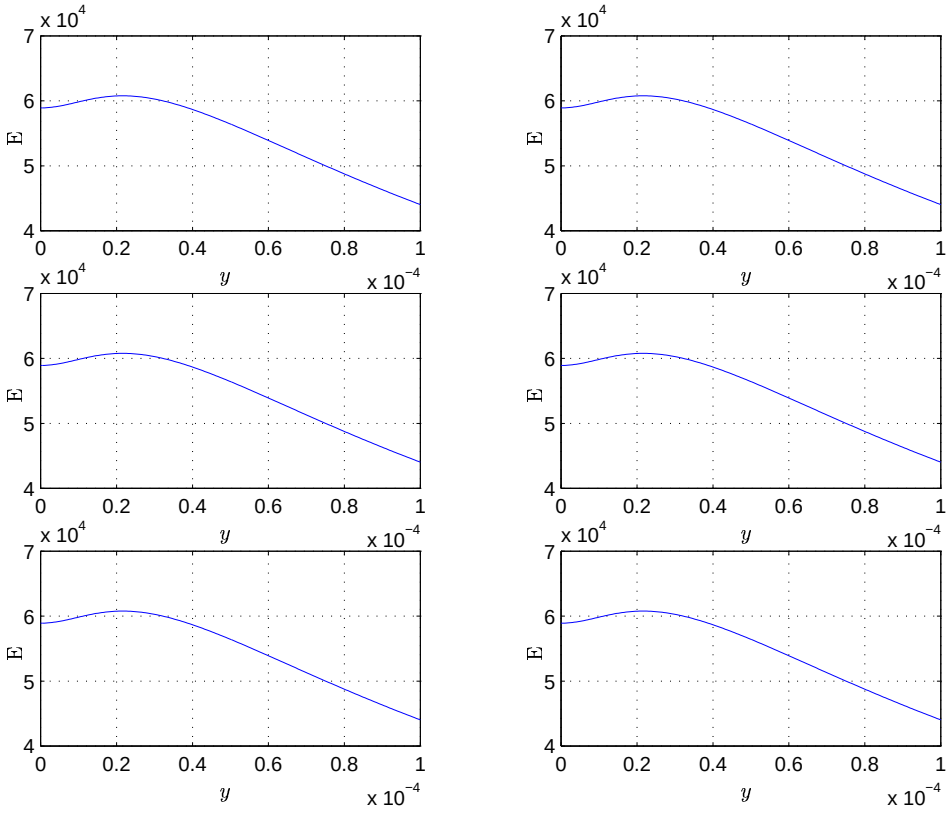


Figure 5.6: Behavior of the electric field ($x$ variation) away from the line charges

Now, keep the $x$ coordinate fix and observe the field behavior by varying $z$ coordinate. Figure 5.7 shows the field distribution changes drastically and is

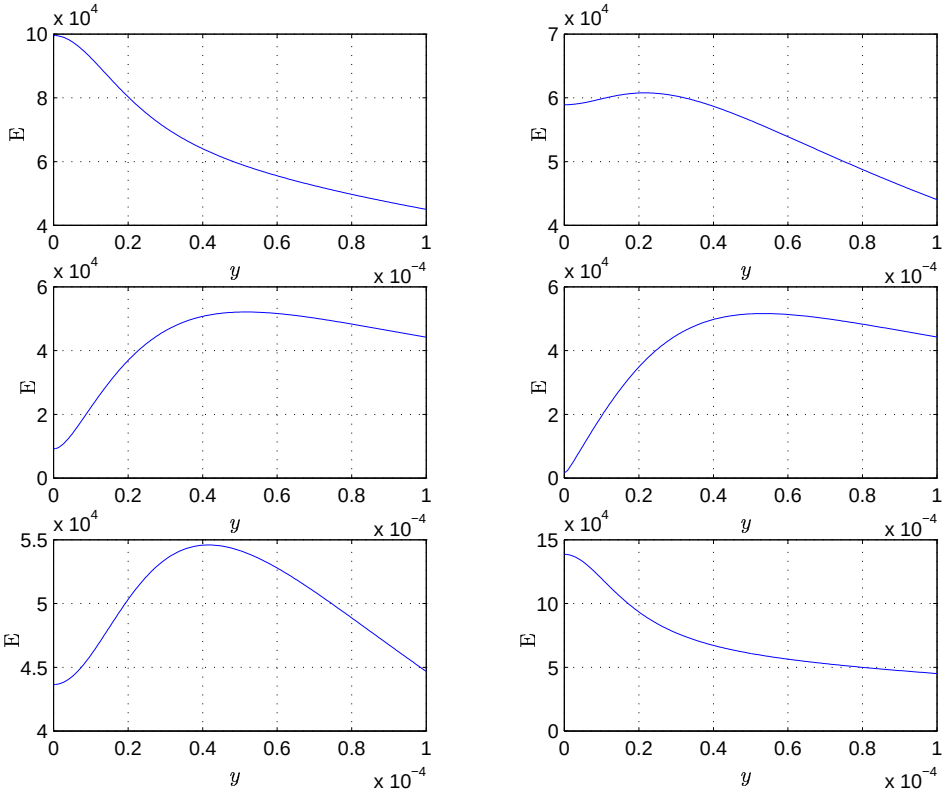


Figure 5.7: Behavior of the electric field (z variation) away from the line charges

qualitatively different to the distribution which we have found out by varying $x$ coordinate. This gives an indication that the reason behind the complicated field behavior out of the model filter depends on the initial measuring point at the plane.

We have seen this behavior at one side of the plane. To have a clear understanding, we observe the field behavior across the plane in $y$ direction. Figure 5.8 shows that the field strength increases continuously as we approach the plane. But for some starting points, near to the plane, it decreases till we leave the plane. In principle, the field reduces to zero at the points where the charge distribution is symmetrical.

We can formulate the above observation mathematically for the simple case of two line charges. Consider an arbitrary point $P(0, y, 0)$ on the $y$ axis. If the length of the line is comparatively bigger than the distance of the point

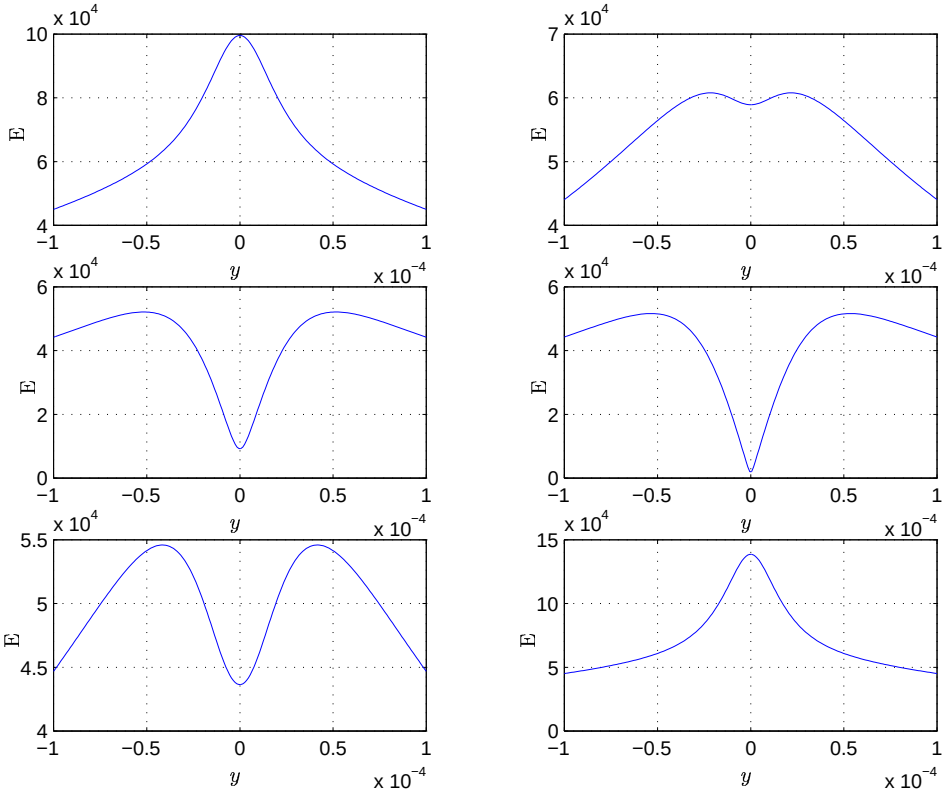


Figure 5.8: Behavior of the electric field across the plane

$P$ from the plane, then the field at $P$ can be approximated as the field due to infinite line charge. Let $2a$ be the distance between the line charges. The unit vectors in the direction of $y$ and $z$ are denoted by $\mathbf{i}$ and $\mathbf{j}$ respectively. The electric field at $P$ can be evaluated as,

$$E = \frac{2k\lambda}{|\mathbf{i}y + \mathbf{j}a|}.\frac{(\mathbf{i}y + \mathbf{j}a)}{|\mathbf{i}y + \mathbf{j}a|} + \frac{2k\lambda}{|\mathbf{i}y - \mathbf{j}a|}.\frac{(\mathbf{i}y - \mathbf{j}a)}{|\mathbf{i}y - \mathbf{j}a|},$$

the above expression can be simplified as,

$$E = \frac{4ky}{(a^2 + y^2)}\mathbf{i} \tag{5.1}$$

Clearly, the behavior of the electric field in equation (5.1) is same as we get in case of model filter.

## 5.3 Electric field at the position of a moving particle

In order to understand the phenomenon observed in the last section, we made a simulation in which a negatively charged polarizable particle starts away from the geometrical center of the spacing between the fibers (Figure 5.10) to the filter. Simulation has been done on both the filter models discussed above.

Coulomb force (electric field) always attracts the particle towards the fibers, although the behavior of the force due to polarization is quite different. Force due to polarization depends on the gradient of the field. $x$ and $z$ components of the force compel the particle to the fibers, whereas $y$ component drives the particle towards the filter plane. Figure 5.9 shows the variation in the $y$ component of gradient of $E^2$ along $y$ direction.

Followings are the main observations: -

- It is clear that until the particle enters in the filter, the gradient remains always negative for extended model, though it is positive initially and then negative for the primary model.
- The particle feels a repulsive force very near to the filter plane in both the cases.
- In both the simulations gradient is positive as the particle leaves the filter. it means that a repulsive force acts at the leaving time.
- The repulsive force increases with increasing surface charge density. Evidently, particle needs more initial velocity to enter in the filter at higher surface charge density.
- The different behavior of gradient for the two models can be explained as, in case of primary model the geometrical center is local, i.e. more charge lies on the one side of the filter whereas in extended filter charge is fully distributed in all the direction around the center. In extended case, the field is minimum at the geometric center, and it always goes down till the center point.

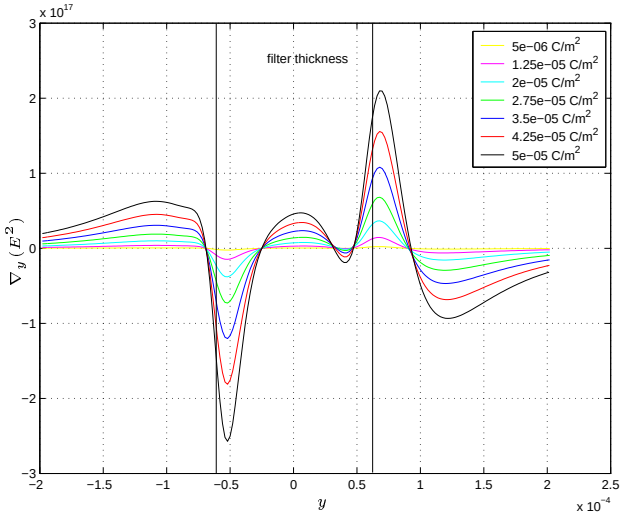


(a) Primary model

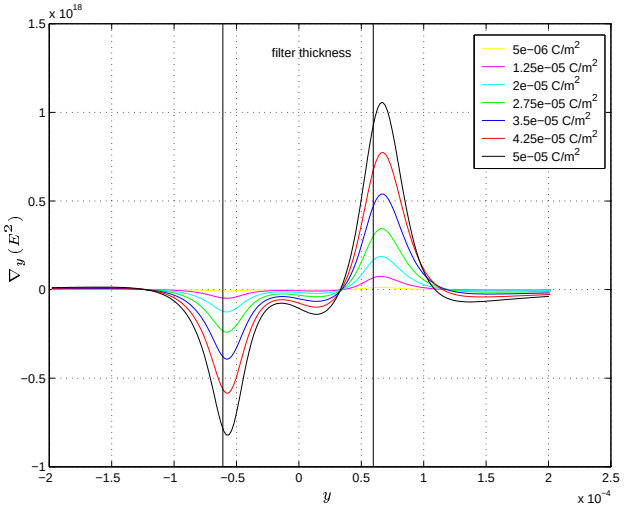


(b) Extended model

Figure 5.9: Variation in $\nabla(E^2)$ with particle motion for different surface charge densities of fibers. Note that due to the motion of the particle the values of x and z can be different at the same value of $y$ for different surface charge densities

## 5.4 Minimum penetration velocity

Our aim is to calculate a critical initial velocity of the particles below which only 5% of the particles can pass through the filter. The simulation with large number of particles to get the minimum penetration velocity was time consuming. In order to get an estimation of this velocity, simulation was done with one particle. A problem arises in choosing the initial position of the particle as the minimum penetration velocity also depends on the initial position. We choose the geometrical center of the spacing between the fibers as initial position, shown in the Figure 5.10. Intuitionally one can expect that the particle passing through the geometrical center needs minimum velocity to cross the filter.

The justification of this phenomenon was done with a simulation for 20 particles with velocity less then the minimum penetration velocity. As expected, 19 particles were trapped out of 20 particles. This gives us a rough confirmation about the fact that we get a maximum trapping efficiency with a velocity less than minimum penetration velocity.

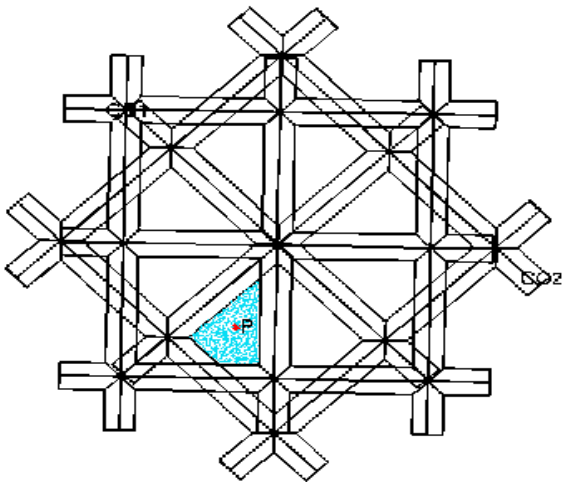


Figure 5.10: Geometric center of spacing between fibers in the model filter

# Chapter 6

# Numerical results

This chapter concerns with the numerical simulation of the particle motion under the influence of the flow field of air and the electric field produced by charged fibers. Filtration efficiency for several surface charge densities of filter fibers has been simulated. Changes in the filtration efficiency with changing particle size have been demonstrated quantitatively. Increment in the efficiency with increasing surface charge density and particle sizes is well described. Minimum penetration velocity of the particles is shown for different charge densities. Variations of minimum penetration velocity with varying particle size are discussed. Practical application of the entire simulation work is also summarized. Results obtained using two different models have been explained in detail. In the simulation, the fibers and the particles have positive and negative charges respectively.

Two types of simulation have been described in the previous chapter. In primary simulation, electric field is calculated by approximating the cylinders as line charges whereas in extended simulation, more line charges are added in primary model until the field converges. Airflow field is calculated over the cylindrical model in both the filters.

In order to determine the relationship between surface charge density, particle diameter, and filtration efficiency, we want to have a large number of particles in the simulation, since the behavior of the field and the structure of the filter are very complicated. Simulation time drastically varies with number of aerosol particles considered in the simulation. For the simulation of particle motion we require the velocity of air and the electric field at the particle position in each step of the motion. The velocity field of air is given at 41830 different grid points in the domain. The velocity at the particle position is approximated by the velocity of the nearest grid point and the

electric field is calculated at that position. The reason behind taking two different models for simulation was due to the fact that the primary model takes less time compared to that of that of the extended model. The qualitative behavior of this disparity is shown in the later context.

Simulation was carried out with 200 aerosol particles starting from random initial positions with same initial velocity. It is assumed that a particle gets deposited if it touches the fiber. Deposition of particle in a simulation filter is shown in Figure 6.1. The collection efficiency extremely depends on initial velocity of the particles. If less number of particles are considered in the simulation then it is difficult to predict the dependency of the initial velocity on the efficiency. In that case it depends on the initial positions of the particles.

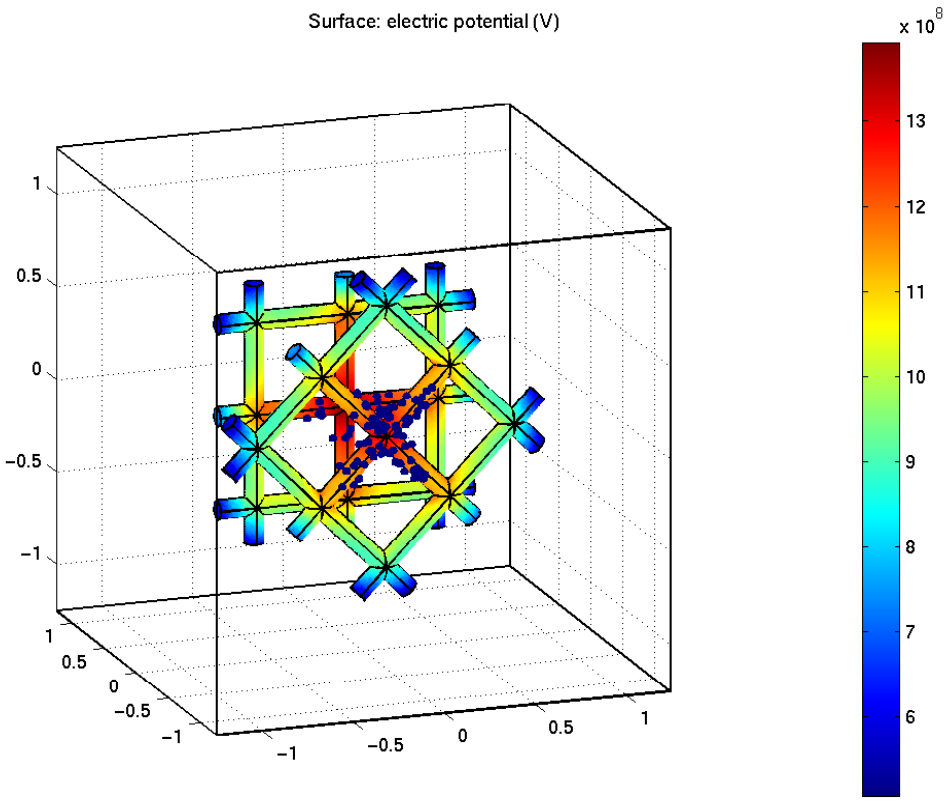


Figure 6.1: Accumulation of particles on simulation filter

## 6.1 Penetration velocity by surface charge density

Figure 6.2 and Figure 6.3 show the dependency of the penetration velocity on surface charge density and on the particle size for both the models. Figures visualize the following findings,

- Minimum penetration velocity increases as a function of surface charge density for charge particles as well as for charged polarized particles.
- The value of the minimum penetration velocity for charged polarized particles is always more than that of simply charged particles. In case of polarization the particle experiences a force $\mathbf{F}_p$ (due to polarization) in addition to a force $\mathbf{F}_c$ (coulomb force), whereas only $\mathbf{F}_c$ is responsible for the motion of the charged particles.
- We have repeated the simulation for different particle sizes and observe that the value of minimum penetration velocity depends systematically on the particle size. The value of penetration velocity decreases with increasing particle diameter.
- Dependence of penetration velocity on the surface charge density are qualitatively same for charge particles and for polarized particles. They both increases in a similar fashion and the curves go nearly together for the particles with smaller diameter. As the diameter of the particles is increased, the curves get apart showing a major difference between the penetration velocities. This differences in penetration velocities are more pronounced for higher charge density as we increase the size of the particle since $\mathbf{F}_p$ (force due to polarization) is more prominent than $\mathbf{F}_c$ (coulomb force) for larger particles as well as for higher surface charge density.

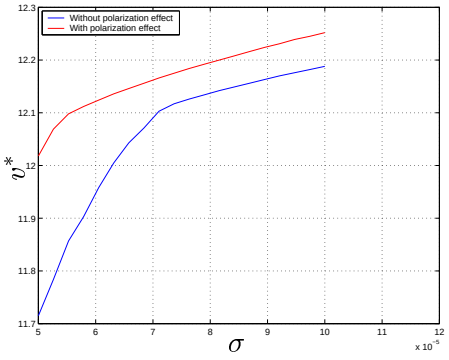


(a) Aerosol particle radius $1\,\mu m$

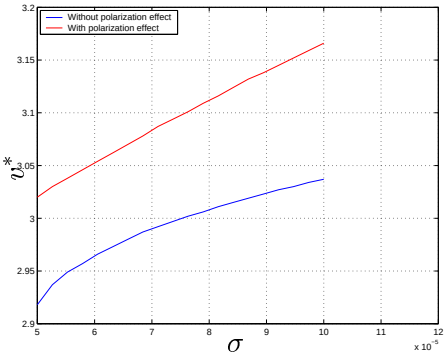


(b) Aerosol particle radius $2\,\mu m$

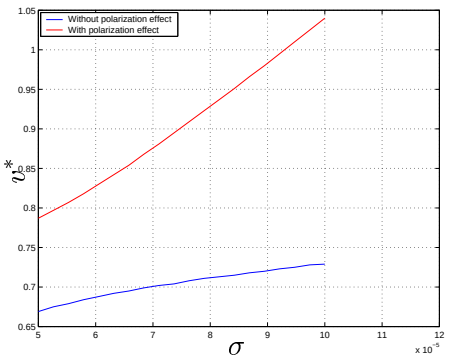


(c) Aerosol particle radius $4\,\mu m$

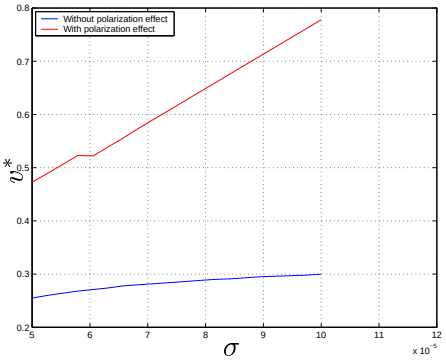


(d) Aerosol particle radius $6\,\mu m$

Figure 6.2: Minimum penetration velocity $v^*$(m/s) vs. surface charge density $\sigma(C/m^2)$ of the fibers for polarizable particles and nonpolarizable particles of different sizes. (Primary model)

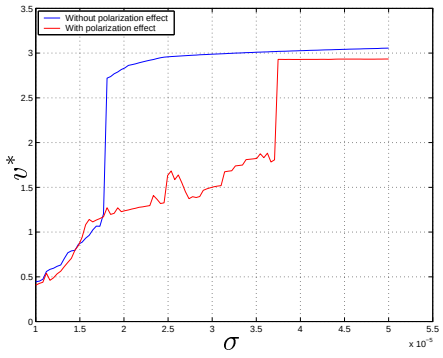


(a) Aerosol particle radius $2\,\mu m$

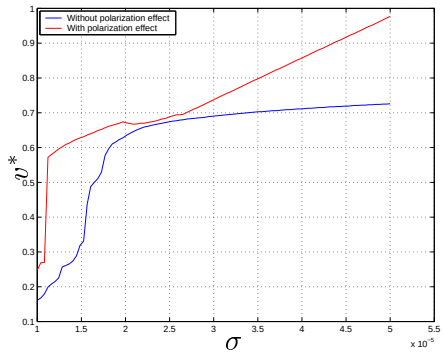


(b) Aerosol particle radius $4\,\mu m$

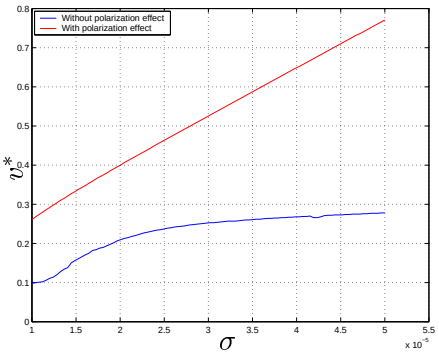


(c) Aerosol particle radius $6\,\mu m$

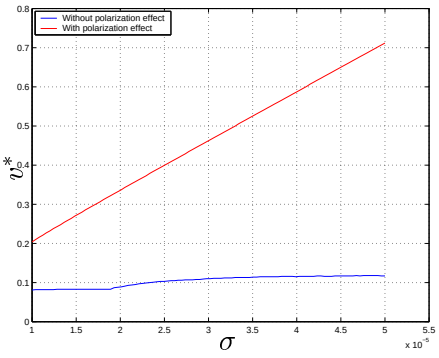


(d) Aerosol particle radius $8\,\mu m$

Figure 6.3: Minimum penetration velocity $v^*$(m/s) vs. surface charge density $\sigma(C/m^2)$ of the fibers for polarizable particles and nonpolarizable particles of different sizes (Extended model).

## 6.2 Filtration efficiency by surface charge density

Filtration efficiency has been observed as a function of surface charge density for different particle sizes in Figure 6.4. The major findings are,

- Filtration efficiency increases with surface charge density.
- Efficiency highly depends on the size of the particle passing through the filter. Efficiency for the bigger particles increases with a slower rate than the smaller particles.
- For lower charge densities, efficiency greatly varies with increasing particle size, whereas for higher charge densities the efficiency essentially become constant, independent of particle size.
- From an application point of view, the results obtained are highly significant. The maximum filtration efficiency can be obtained by inducing a higher value of a surface charge density. From the figure, it is clear that by fixing the surface charge density, a value more then $15\mu C/m^2$, one can achieve the maximum efficiency independent of particle size shown in the figure. It is also evident immediately that the filter with lower charge density attains the maximum filtration efficiency for the particles with radius more then $9\mu m$.

## 6.3 Filtration efficiency by particle size

A qualitatively study of the filtration efficiency can be made with the knowledge of particle size distribution and surface charge density. Figure 6.5 shows the filtration efficiency with particle diameter over a range of surface charge density. It is clearly evident from the figure that a saturation point in the filtration efficiency is obtained beyond a particle diameter.

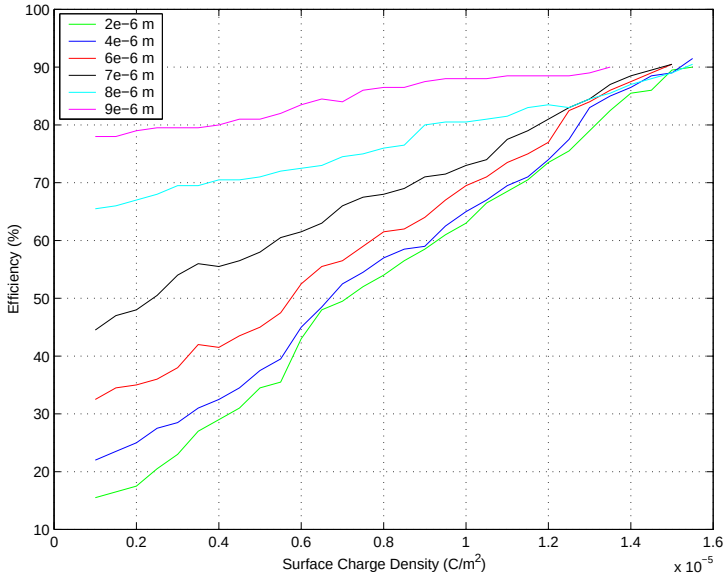


(a) Primary model

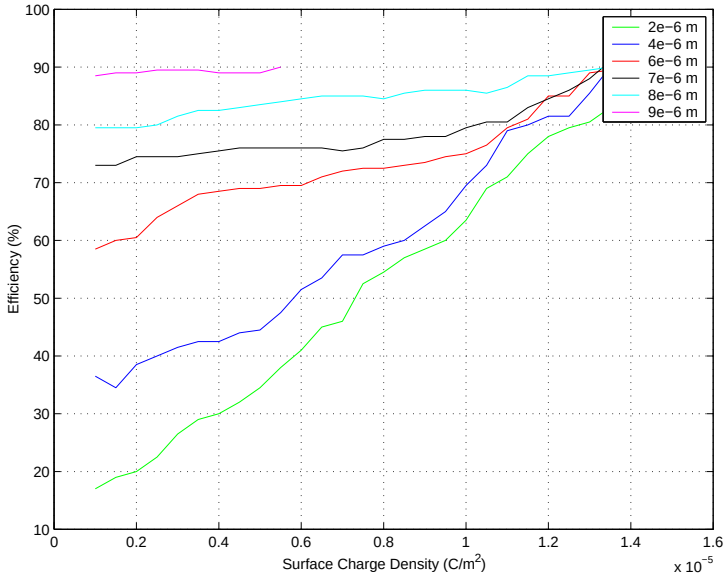


(b) Extended model

Figure 6.4: Filtration efficiency vs. surface charge density for various particle radiuses

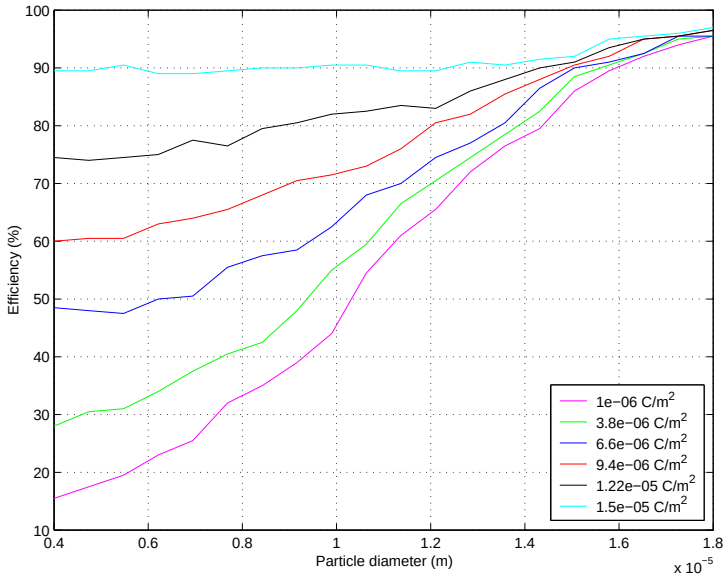


(a) Primary model

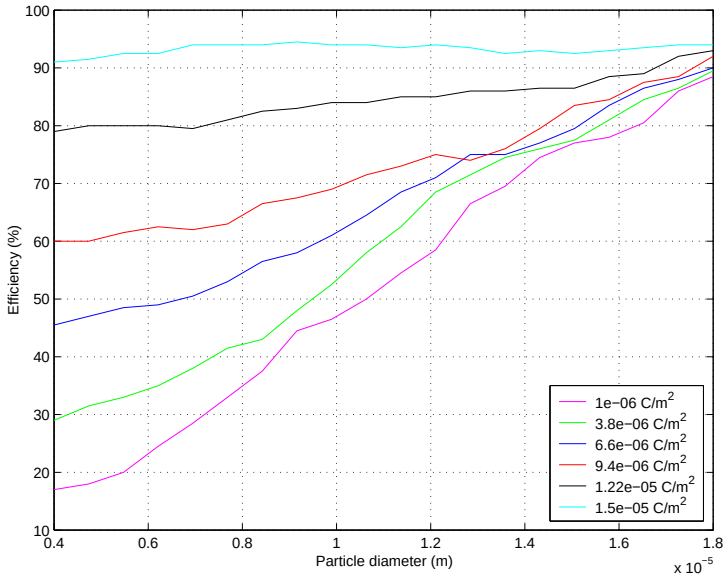


(b) Extended model

Figure 6.5: Filtration efficiency vs. particle diameter over a range of surface charge density

# Chapter 7

# Conclusions

In this work, the filtration process through a charged filter is studied. The flow through the filter has been calculated by using the steady state stokes flow formulation. The electric field of the filter geometry has been calculated numerically by solving the static Maxwell equations. In addition, an analytical solvable model for the electric field of the filter has been formulated. The size dependence of the electric field has been studied with an analytical approximation. A strong dependence for small to medium filter sizes was found, but it could be prove that there is a finite limit of the electric field for infinite filter size. A comparison of numerical and analytical results is included, which confirms the reliability of analytical formulation. The behavior of the electric field across the filter has been obtained. The nature of the particle motion is described in terms of the interaction of particle with the existing electric field and the airflow field. The effects of increasing surface charge density and particle size on filtration efficiency have been simulated for two models. The minimum passing velocity, i.e., the minimum velocity of a particle to leave the filter again after entering it, has also been analyzed as a function of increasing surface charge density and increasing particle size.

# Bibliography


[1] Davies, C. N. (1949) Fibrous filters for dust and smoke, in *proc. 9th Int. Congress on Ind. Med.,* Simpkin Marshall, London, 162-196.

[2] Elsevier (1995) *Profile of the Worldwide Filtration and Separation Industry,* Elsevier Advanced Technology, Elsevier, Oxford.

[3] Fuchs, N.A. and Stechkina, I.B. (1963) *Ann. Occup. Hyg.,* 6, 27-30.

[4] Natanson, G. (1957b) Deposition of aerosol particles by electrostatic attraction upon a cylinder around which they flowing, *Dokl. Akad. Nauk USSR,* 112, 696-699.

[5] Havlicek, V. (1961) The improvement of the efficiency of fibrous dielectric filters by application of external electric field, *Ont. J. Air Water Pollut.,* 4, 225-336.

[6] Landau, L.M. and Lifshitz, E.M. *Electrodynamics of Continuous Media*, Pergamon Oxford, 1960.

[7] Panofsky, W.K.H. and Philips, M. *Classical Electricity and Magnetism,* 2nd edition, Addison-Wesley, Reading, Mass.,1962.

[8] Jackson, J.D. *Classical Electrodynamics,* John Wiley & Sons Inc.,1975.

[9] Wilfred Kaplan *Advanced Calculus,* Addison Wesley, 1973.

[10] Curle, N. and Davies, H.J. *Modern Fluid Dynamics,* Van Nostrand Reinhold Company London, 1968.

[11] Kvestoslav R. Spurny *Advanced in Aerosol Filtration,* Lewis Publishers, 1998.

[12] Halliday, D. and Resnick, R. *Fundamentals of physics,* John Wiley & Sons Inc.,1970.

[13] Tritton, D.J. *Physical Fluid Dynamics,* Van Nostrand Reinhold Company London, 1977.

[14] Clyde Orr *FILTRATION Principles and Practices,* Marcel Dekker, Inc., 1977.

[15] Christopher Dickenson, FBIM *Filters and Filtration,* Elsevier Advanced Technology, 1992.

[16] Brown, R.C. *Air Filtration,* Pergamon Oxford, 1993.

[17] Batchelor, G.K. *An Introduction to Fluid Dynamics,* Cambridge University Press, 2000.